



Article

Thermo-Mechanical Fatigue in AISI 347 Austenitic Stainless Steel: Phase Transformation Kinetics at Elevated Temperatures

Viktor Lyamkin ^{1,*}, Sascha Power ², Christian Boller ² and Peter Starke ^{1,2}

- Department of Materials Science and Materials Testing, University of Applied Sciences, 67659 Kaiserslautern, Germany; peter.starke@hs-kl.de
- Department of Non-Destructive Testing and Quality Assurance, Saarland University, 66123 Saarbrücken, Germany; saschadirk.power@uni-saarland.de (S.P.); c.boller@mx.uni-saarland.de (C.B.)
- * Correspondence: viktor.lyamkin@hs-kl.de; Tel.: +49-631-3724-2043

Abstract

Thermo-mechanical fatigue remains one of the more difficult phenomena to analyze due to the interplay between temperature, mechanical properties, and microstructural features of the material. For austenitic stainless steel, thermo-mechanical fatigue plays a particularly critical role—temperature changes the affinity of γ austenite to transform into α' martensite under overcritical deformation. This paper presents the results of an in situ study of $\gamma \to \alpha'$ deformation-induced transformation kinetics at elevated temperatures in AISI 347. Fatigue tests were conducted in the temperature range of 20 to 320 °C. A uniaxial magnetic balance was used to directly measure the change in ferromagnetic volume fraction of the fatigue specimens as the fatigue load was applied. From this data, an empirical mathematical model was found. This model describes the kinetics of $\gamma \to \alpha'$ transformation as an exponential function of temperature, where the rate of phase transformation decreases with temperature, asymptotically approaching zero but never actually reaching it.

Keywords: martensite; deformation-induced; thermo-mechanical; fatigue; magnetic; evaluation; stainless steel; austenite; non-destructive testing



Academic Editor: Alberto Campagnolo

Received: 15 August 2025 Revised: 3 September 2025 Accepted: 13 September 2025 Published: 16 September 2025

Citation: Lyamkin, V.; Power, S.; Boller, C.; Starke, P. Thermo-Mechanical Fatigue in AISI 347 Austenitic Stainless Steel: Phase Transformation Kinetics at Elevated Temperatures. *Appl. Sci.* 2025, 15, 10095. https://doi.org/10.3390/ app151810095

Copyright: © 2025 by the authors. Licensee MDPI, Basel, Switzerland. This article is an open access article distributed under the terms and conditions of the Creative Commons Attribution (CC BY) license (https://creativecommons.org/licenses/by/4.0/).

1. Introduction

One of the challenges in characterizing the thermo-mechanical $\gamma \to \alpha'$ transformation process under fatigue loading is the combination of elevated temperatures with fairly low strain amplitudes. This combination of a low α' volume fraction with the difficulty of measuring magnetic properties at elevated temperatures while applying mechanical deformation to the material creates difficult conditions for experimental evaluation.

AISI 347 (X6CrNiNb18-10, 1.4550) is a metastable austenitic stainless steel often used in piping and structural components of nuclear power plants. Being metastable, it can undergo a phase transformation from paramagnetic γ austenite into ferromagnetic α' martensite. This transformation may happen in two ways: by cooling it down to the martensite start temperature M_s or by mechanical deformation [1,2]. The higher the temperature, the more mechanical deformation is required for $\gamma \to \alpha'$ transition to occur.

In 1979, Cohen, Olson, and Clapp defined martensitic transformation within a wider class of displacive (diffusionless) transformations as "shear dominant, lattice distortive, diffusionless transformation occurring by nucleation and growth" [3]. Experimental investigations later showed that plastic deformation of γ austenite can lead to (I) direct transformation to α' martensite; (II) transformation into ε martensite; or (III) transition to α' via a transient ε phase [4].

Direct $\gamma \to \alpha'$ transformation was first described by Bain [5]. Bain's model shows how a simple distortion allows a face-centered cubic (fcc) lattice to be transformed into a body-centered cubic (bcc) lattice with an intermediate tetragonal distortion. Several other models have been proposed to describe the $\gamma \to \alpha'$ transformation, including Kurdjumow and Sachs [6], Nishiyama [7], Pitsch [8], and Bogers and Burgers [9].

If T_0 is considered the temperature at which martensite and austenite are in thermodynamic equilibrium, then at temperatures above T_0 , austenite is the more energetically favorable phase, while below T_0 , α' martensite is more favorable. The transition from γ to α' does not happen exactly at T_0 . It is necessary to undercool austenite to the martensite start temperature M_s to initiate the thermal $\gamma \to \alpha'$ transition [2]. This delay is due to the existence of non-chemical energy barriers such as interfacial and elastic energy [10]. This means that a critical driving force is needed to initiate the martensitic transformation. This critical force corresponds to the chemical free energy difference ΔG_{min} ,

$$(\Delta G_{therm} + \Delta G_{mech}) \ge \Delta G_{min} \tag{1}$$

between undeformed austenite and α' martensite at the M_s temperature, where the transformation occurs without any additional external energy. When a load is applied to the material, ΔG_{mech} increases. This means a smaller gap between ΔG_{therm} and ΔG_{min} is needed to reach the critical amount of free energy.

It was noted by Hansel [11] that the amount of deformation-induced martensite ξ as a function of strain can generally be characterized by Figure 1. Three sections can be distinguished based on the rate of phase transformation: (I) accelerated rate; (II) constant rate; (III) decelerated rate. It was demonstrated by Smaga [12] that the kinetics of cyclic strain also follow a similar curve. There are certain simplifications that were implemented in this work: two linear ranges were defined. LR1 corresponds to the highest rate of phase transformation, and LR2 is the rate of phase transformation near saturation, where most of the austenite has already transformed.

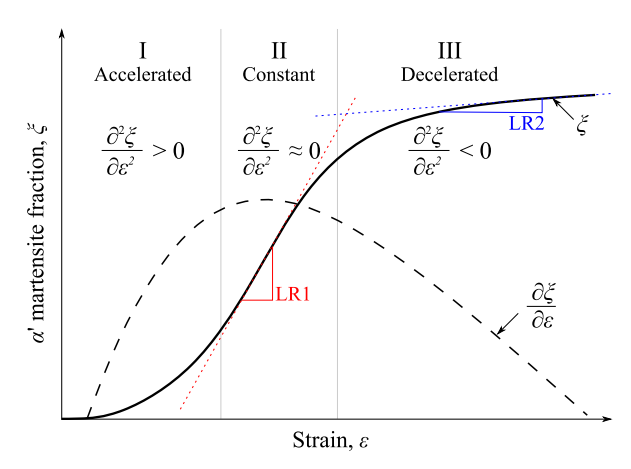


Figure 1. The typical development of deformation-induced martensite as a function of strain: (I) accelerated rate; (II) constant rate; (III) decelerated rate. The solid line shows the amount of deformation-induced martensite, while the dashed line shows the rate of phase transformation.

Estimating the remaining fatigue life based on the amount of α' martensite would be relatively straightforward if the operational temperature of the component remained constant. Unfortunately, this is rarely the case. For AISI 347, the formation of α' martensite is significantly reduced above 100 °C, and it is generally accepted that no phase transformation takes place at the temperatures of a pressurized water reactor of about 320 °C. However, there is experimental evidence [13] that $\gamma \to \alpha'$ transformation still occurs at these temperatures, but in extremely small quantities.

In this study, these small quantities of deformation-induced martensite have been experimentally measured, which allowed some conclusions to be drawn about phase transformation kinetics at elevated temperatures.

2. Materials and Methods

This work features several testing and measurement methods that have been developed at Saarland University and are now also being used at the University of Applied Sciences Kaiserslautern. These methods include uniaxial magnetic balance and magnetic force imaging. Ohmic heating of the fatigue specimen was realized by a step-down transformer with multiple primary taps connected to a PID controller. Fatigue testing was conducted under total strain control, with constant and step-wise increasing amplitudes.

2.1. Magnetic Methods

Two magnetic measurement methods have been used during this study: a uniaxial magnetic balance (UMB) and magnetic force imaging (MFI).

The UMB is a magnetic balance consisting of two permanent magnets mounted on one axis. The force between the magnets is measured by two load cells and calibrated to the ferrite volume fraction based on standard calibration samples, provided by Helmut Fischer GmbH, originally meant for Feritscope [14]. Fatigue specimens were placed in such a manner that the gauge length is centered between the two magnets. This initial alignment was performed by moving the entire UMB with a micrometer screw until the force readout from both load cells became equal. The UMB system enabled in situ detection of small fractions of deformation-induced martensite during fatigue loading. The resolution of the UMB in offline measurements can exceed 0.01 Fe%, while for in situ measurements, the resolution was affected by the heating current, as well as the mechanical movement of the fatigue specimen. Further information about the UMB can be found in [15].

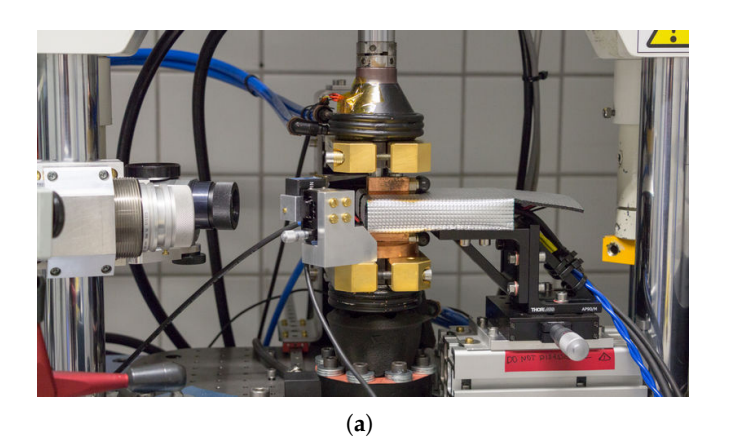
MFI is a scanning technique where the force interaction between a permanent NdFeB magnetic tip and a sample is measured. The magnetic tip used in this study had a diameter of 0.3 mm, and most of the scans were performed at a working distance (WD) between 10 and 20 μ m. The imaging process was realized by line scanning in XY coordinates at a constant speed of 0.4 mm/s. Scanning started with a fast trace line (6 mm/s), where no data were acquired. This step was taken to pre-magnetize the material for the retrace line, where the force response is measured, and also to avoid possible backlash in the actuators. After the retrace is complete, the Y-stage moves the sensor to the next line. As a result, data are obtained only in one direction of scanning. The typical spatial resolution of a scan is 0.05 mm. The lateral resolution is strictly limited by the magnetic tip diameter and is dependent on the working distance. In this work, it can be estimated to be between 0.3 and 0.5 mm. To be analyzed with MFI, fatigue specimens were cut with electric discharge machining (EDM) in the axial direction, embedded in resin, ground, and polished to 1 μ m with a diamond suspension. Further information about MFI can be found in [16].

2.2. Thermo-Mechanical and Elevated Temperature Fatigue Testing Rig

In order to realize in situ magnetic measurements with the UMB, it is essential to have a sufficient amount of space around the fatigue specimen. A solution was found in a system that passes alternating current up to 800 A at 50 Hz frequency through the specimen. It has been built around a commercial 20 kN Servopulser servo-hydraulic fatigue testing machine (Shimadzu Deutschland GmbH, Duisburg, Germany) as illustrated in Figures 2 and 3.

The fatigue specimen was gripped by current injection clamps, which had been goldplated to improve electrical contact. These clamps were then attached to the water-cooled grips of the fatigue machine. The load cell of the fatigue machine was electrically insulated from the

rest of the frame to prevent current leakage. The current was supplied by a custom-made mains transformer with multiple primary windings and a single high-current secondary winding. The voltage output was regulated by a PID controller through a solid-state tap changer.



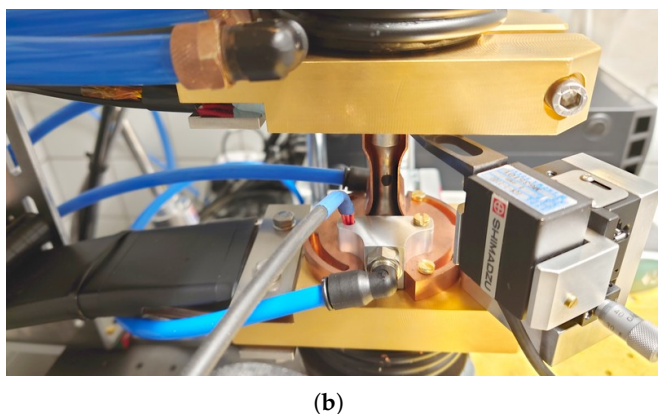


Figure 2. Views of the fatigue specimen mounted in the TMF testing rig: (a) front view with the UMB placed in the measurement position; (b) side view without the UMB, showing the fatigue specimen under the heat shield.

A heat shield, machined from a single copper block, was used to protect the UMB from extreme temperature changes. The heat shield geometry follows the shape of the fatigue specimen and allows unobstructed access for the UMB. To maintain a stable temperature, the grips and the heat shield were continuously water-cooled with 15 $^{\circ}$ C water.

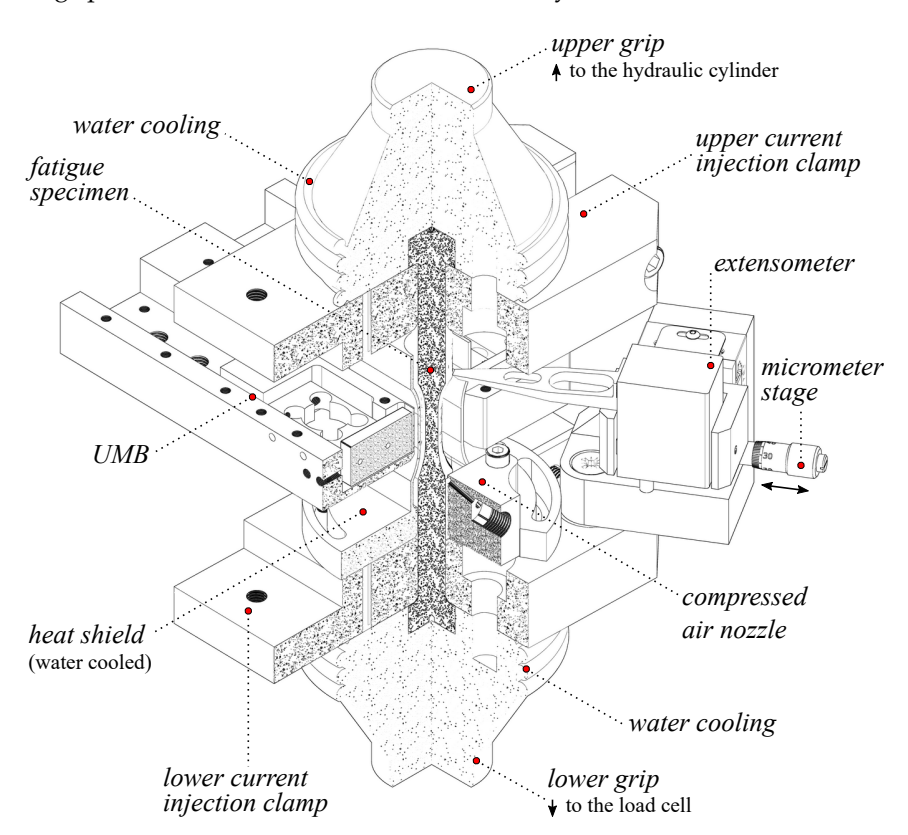


Figure 3. Schematic representation of the thermo-mechanical and elevated temperature fatigue testing rig.

A CellaTemp PA 10 pyrometer with a thermopile sensor from Keller HCW GmbH (Ibbenbüren, Germany) was used to monitor the fatigue specimen temperature. The pyrometer was placed at a distance of 155 mm from the pyrometer lens to the specimen

surface. At this distance, the field of view of the pyrometer is 3.23 mm in diameter, which is appropriate for 6 mm diameter fatigue specimens. The measuring range of this pyrometer spans from 0 to 1000 °C, which corresponds to a wavelength of 14 to 8 μ m. Temperature T_c was measured at the center of the specimen gauge length.

An extensometer had been set up to measure the travel between the lower grip and the upper part of the fatigue specimen, as shown in Figure 3. This configuration provided acceptable strain measurement results after calibration was performed with a standard 12 mm gauge length extensometer. This calibration was performed by comparing the amplitudes of the two extensometers in a stress-controlled test. A stress amplitude of around 100 MPa was chosen to remain in the pure elastic regime.

2.3. Material and Specimen Geometry

This study focuses on austenitic stainless steel AISI 347 (1.4550, X6CrNiNb18-10). The unique alloying element of this steel is niobium, which has a higher affinity for carbon than chromium. This prevents the formation of chromium carbides and results in improved resistance to intergranular corrosion. This steel is also considered metastable and undergoes deformation-induced phase transformation from paramagnetic γ austenite to ferromagnetic α' martensite under plastic deformation at room temperature. This change from a paramagnetic to a ferromagnetic state is what has been largely exploited in this work to analyze the phase transformation kinetics.

The raw material was manufactured by means of continuous casting to a square cross-section using an electromagnetic stirring device. It was then hot-rolled to change the cross-section from square to round with a diameter of around 31 mm. In the next step, the material went through solution annealing at a temperature of $1058\,^{\circ}$ C. Final turning to a diameter of 30 mm was performed after cooling. All these steps were performed by the manufacturer, and no additional heat treatment was applied on-site. The chemical composition, as per the manufacturer's certificate, is specified in Table 1. The material was then further machined to the geometry specified in Figure 4. As a final preparation step, specimens were electrochemically polished to reduce the amount of α' martensite that could have formed on the surface due to machining. Measured by the UMB, the initial ferromagnetic volume fraction ζ_{fm} was on average 0.82% for all specimens.

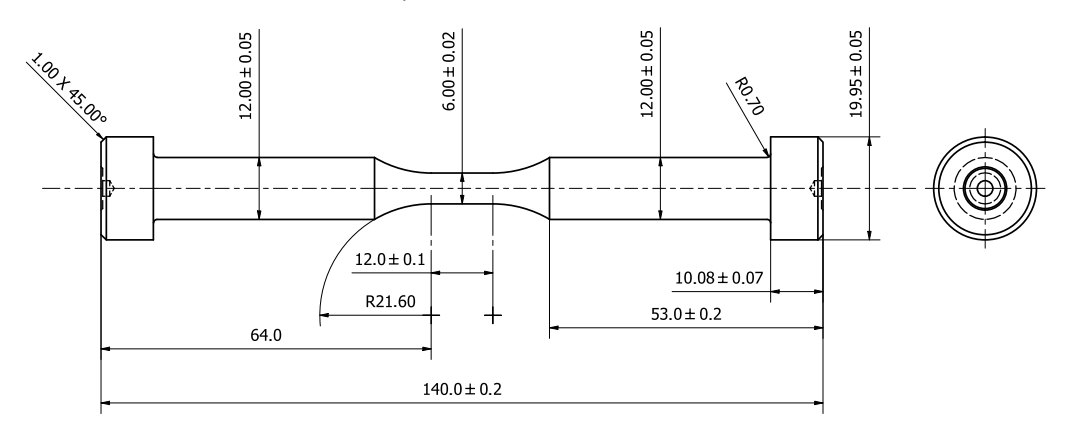


Figure 4. Fatigue specimen geometry. Dimensions in mm.

Table 1. Chemical composition in wt% of AISI 347 used in this study, as specified by the manufacturer. The martensite start temperature M_s and the temperature at which 50% of martensite is formed under 30% strain M_{d30} were calculated in accordance with [17].

С	Si	Mn	Ni	Cr	S	P	Nb	M_s	M_{d30}
0.051	0.409	0.714	9.121	17.165	0.003	0.029	0.547	-47.24	58.08

3. Results

This section presents the results of two experimental approaches:

• Strain increase tests: Evaluation of the strain limit for cyclic-deformation-induced $\gamma \to \alpha'$ transformation;

• Constant strain amplitude tests: Evaluation of $\gamma \to \alpha'$ phase transformation kinetics at elevated temperatures.

3.1. Strain Limit for Cyclic-Deformation-Induced Transformation

The strain increase test (SIT) is a total-strain-controlled fatigue test that starts at a low strain amplitude, which increases gradually in fixed intervals, called steps. A constant strain rate of $0.004~\rm s^{-1}$ and a triangular waveform were chosen to avoid excessive heat generation at lower temperatures. The duration of a single step was equal to 120 min. After every 120 min, the total strain amplitude increased by 0.01%, starting from 0.05%. The results of five SITs are summarized in Figures 5 and 6.

The results showed plastic strain amplitude $\varepsilon_{a,p}$ to be consistently higher at elevated temperatures. At $T_c = 240$ °C, plastic strain was almost twice that at ambient temperature. An indication of cyclic hardening can be identified here as the plastic strain amplitude drops within a single step after $\varepsilon_{a,t} = 0.15\%$. Such behavior could be observed only up to 160 °C. The test performed at 240 °C showed no significant change in plastic strain amplitude within one step. Logically, the lowest stress amplitudes could also be found at 240 °C. From stress amplitudes, signs of cyclic softening could be observed for all temperatures, except 17 °C, in the range $0.11 \le \varepsilon_{a,t} \le 0.16$ (%). After step number 16 at $\varepsilon_{a,t} = 0.20\%$, cyclic hardening could be observed, even at 240 °C, from the increased stress amplitude within a single step. Cyclic relaxation at 80 °C and above could be observed after step 4, $\varepsilon_{a,t} = 0.08\%$, from the decreasing mean stress.

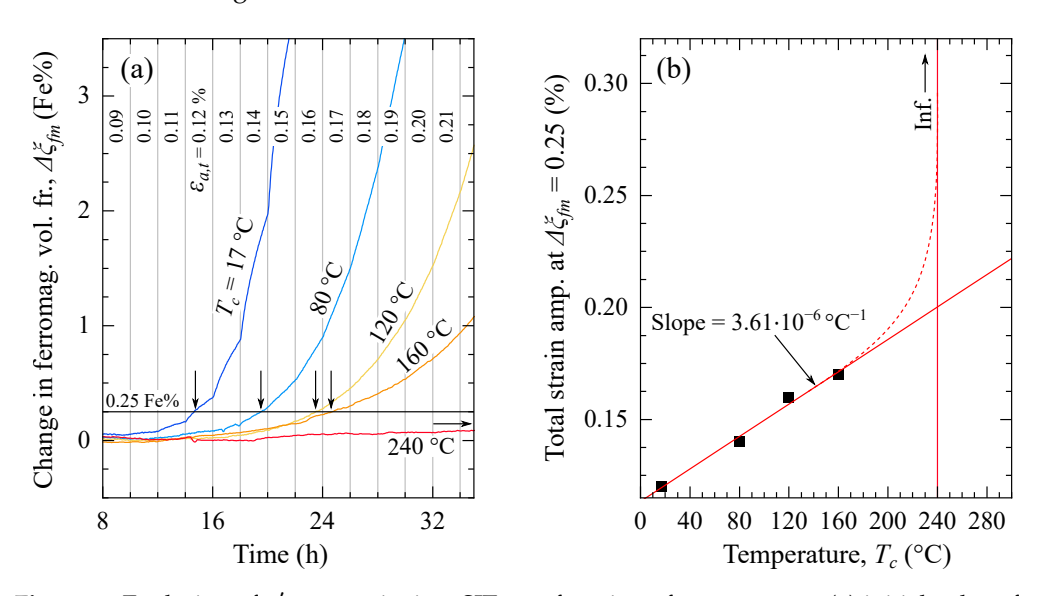


Figure 5. Evolution of α' martensite in a SIT as a function of temperature: (a) initial values from Figure 6 of α' volume fraction in Fe%; (b) total strain amplitude at which 0.25 Fe% was reached for different temperatures.

The initial phase transformation, measured by the UMB, can be seen more clearly in Figure 5a, where the ordinate from Figure 6a is limited to 3.5 Fe%. By convention, a threshold of 0.25 Fe% was selected to visually represent the effect of temperature on the α' content in the strain increase tests (see Figure 5b). At ambient temperature (T_c = 17 °C), phase transformation was observed at a strain amplitude of 0.1%. At about the same strain amplitude, mean stress relaxation could be observed, as shown in Figure 6d. For T_c = 80 °C

and above, stress relaxation was observed earlier, at around 0.08% strain amplitude. Since the SIT at 240 °C resulted in specimen failure before 0.25 Fe% could be reached, a vertical line is plotted in Figure 5b at 240 °C to signify the possibility of M_d being reached.

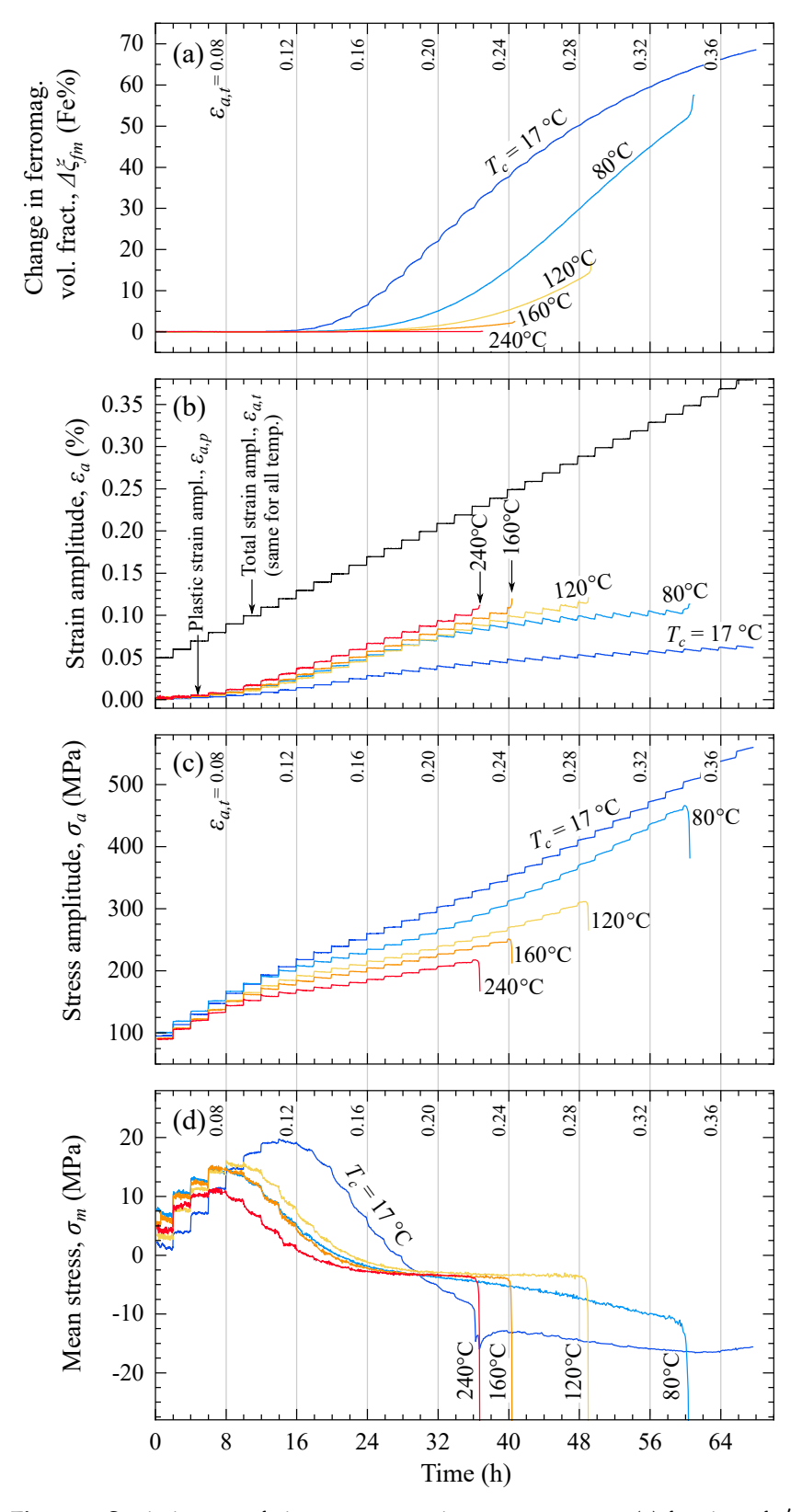


Figure 6. Strain increase fatigue tests at various temperatures: (a) fraction of α' martensite in Fe% with initial values subtracted; (b) total strain amplitude, valid for all temperatures and plastic strain amplitudes; (c) stress amplitude response of the material; (d) mean stress amplitude.

3.2. Phase Transformation Kinetics at Elevated Temperatures

The kinetics of $\gamma \to \alpha'$ transformation were studied in a series of nine isothermal constant strain amplitude fatigue tests, which were performed at the same strain amplitude $\varepsilon_{a,t} = 0.5\%$. Each fatigue test was performed at different specimen temperatures, from $T_c = 17$ °C to 320 °C. Strain was controlled with a sinusoidal function, with a frequency of 0.02 Hz. Figure 7 shows stress–strain hysteresis loops at the beginning of cyclic loading. A clear influence of temperature can already be observed from the increased plastic portion in the hysteresis at elevated temperatures. This effect can be seen better in Figure 8a, where only the initial part of the hysteresis is plotted.

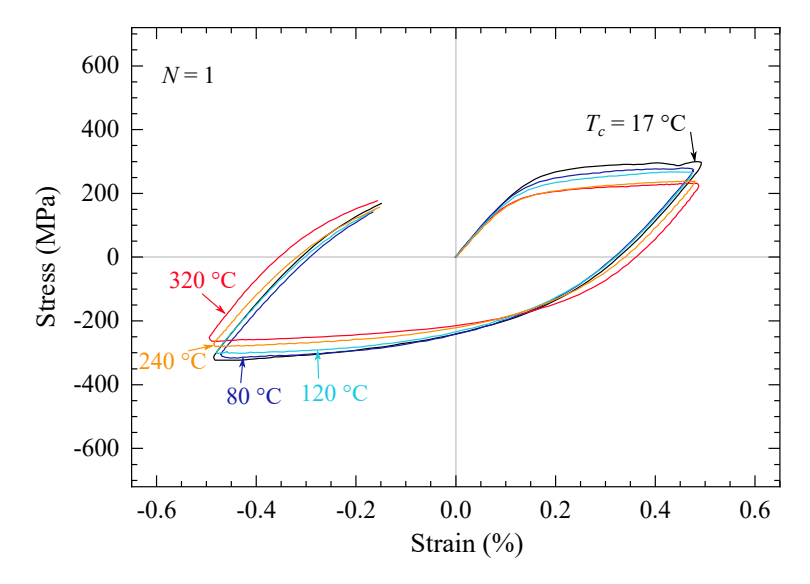


Figure 7. Stress–strain diagram showing the first cycle of constant strain amplitude tests at various temperatures.

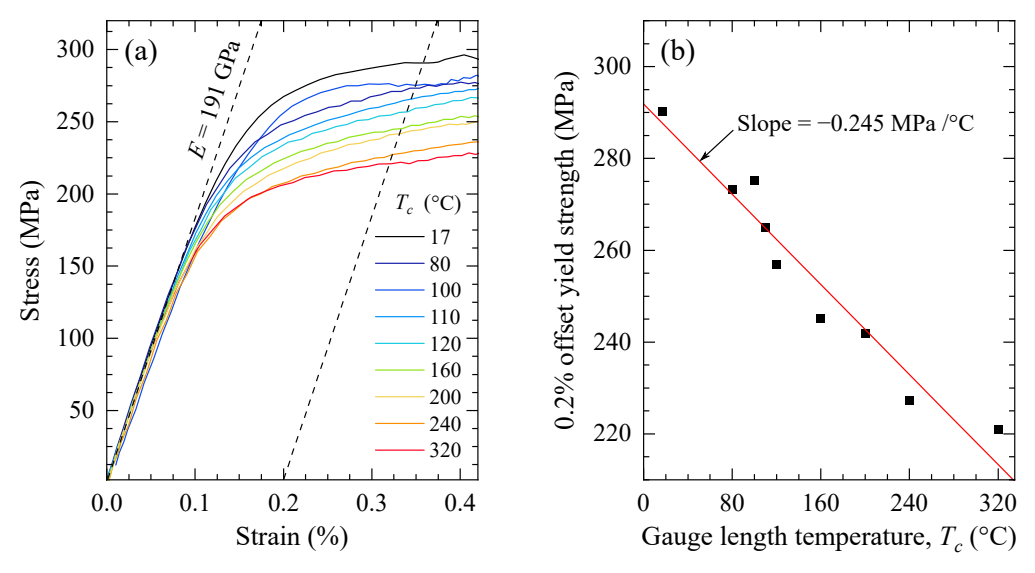


Figure 8. The influence of temperature on the yield strength: (a) the stress–strain diagram generated from the first cycle of isothermal fatigue tests; (b) yield stress as a function of temperature. Yield stress is calculated as 0.2% offset from the elastic slope.

From this figure, Young's modulus was estimated to be 191 GPa, which is in accordance with the manufacturer's report. The elastic portion was found to be nearly identical at all temperatures. In Figure 8b, 0.2% offset yield strength is plotted to further visualize the effect of temperature on mechanical properties. The yield strength appeared to decrease by 0.245 MPa for one degree Celsius. Cyclic hardening behavior can be observed more clearly

at cycle number 800 in Figure 9. Here stress amplitude at ambient temperature was almost 200 MPa higher when compared to 120 $^{\circ}$ C and above. Stress amplitude as a function of the number of cycles is presented in Figure 10.

While cyclic hardening can be used to detect the transformation from austenite to α' martensite, it is not entirely reliable due to dislocation rearrangement and cyclic softening potentially happening at the same time. Magnetic methods, i.e., uniaxial magnetic balance measurements presented in Figure 11, are a more reliable way to quantify the amount of deformation-induced martensite.

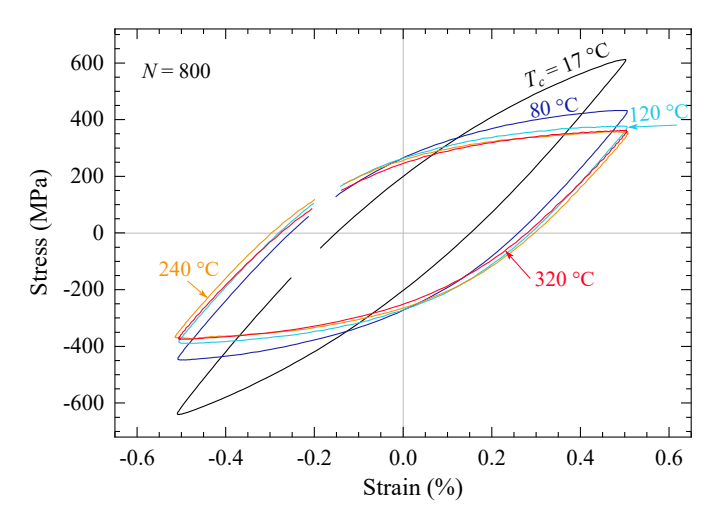


Figure 9. Stress–strain diagram showing the 800th cycle of constant strain amplitude tests at various temperatures.

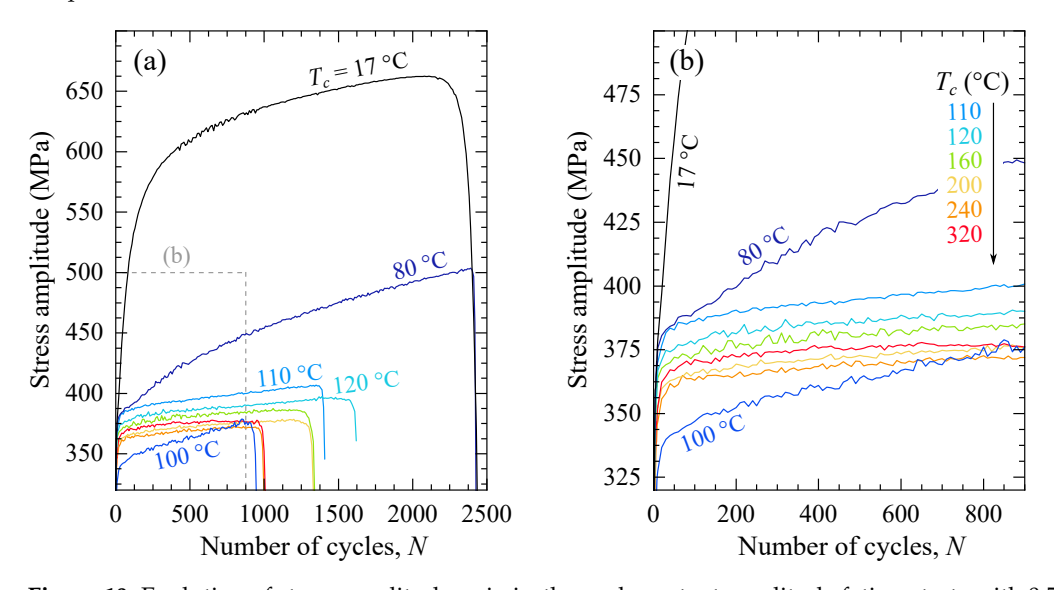


Figure 10. Evolution of stress amplitude σ_a in isothermal constant amplitude fatigue tests with 0.5% total strain amplitude: (a) full range; (b) initial range.

The results of the UMB measurements showed a good correlation between cyclic hardening and the amount of α' martensite. The three regions described in the Introduction, namely, accelerated, constant, and decelerated (see Figure 1), were predominantly observed at lower temperatures. At 80 °C and 100 °C, only accelerated transformation behavior was evident. As the temperature increased, the phase transformation rate became more linear. At 240 °C, only a 0.05 Fe% increase was recorded at the end of the test, and no change in ferromagnetic volume fraction was measured at 320 °C.

In order to simplify the calculation, only the linear range LR1 was considered (see Figure 1), which corresponds to the highest rate of phase transformation. The values that

were used for the calculation are listed in Table 2 and plotted in Figure 12. From this data, a trend can be noticed that can be described by the equation

$$\frac{\partial \xi_{fm}}{\partial N}(T_c) = k \cdot m^{T_c},\tag{2}$$

which describes the rate of ferromagnetic volume fraction ξ_{fm} over the number of cycles N as a function of specimen temperature T_c . In this equation, k and m are the fit parameters. After fitting Equation (2) to experimental data, these coefficients were found to be $k = 2.287 \pm 0.4$ and $m = 0.944 \pm 0.002$. The R^2 value of the fit was 0.93. Parameter m determines how quickly the rate of $\gamma \to \alpha'$ transformation decreases with temperature. Parameter k is essentially a proportionality coefficient.

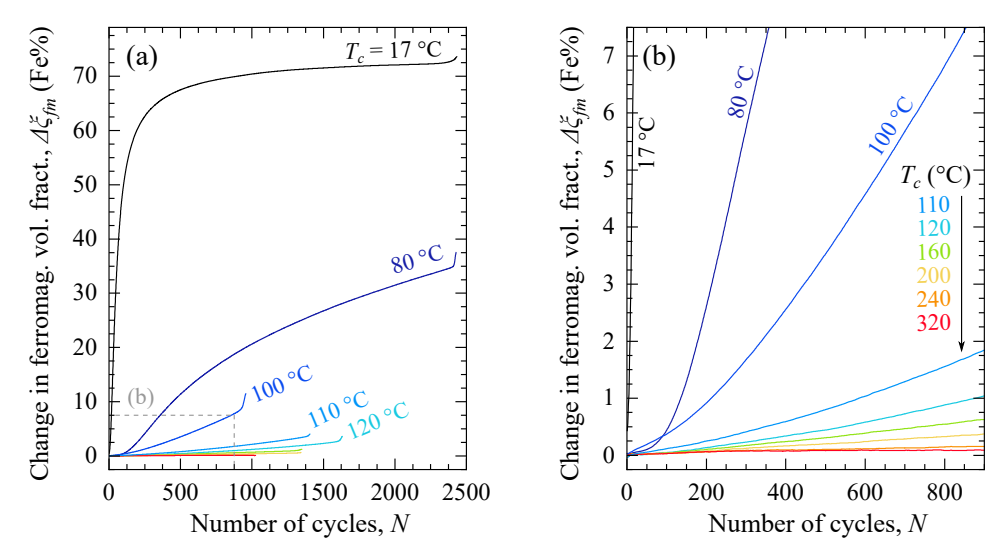


Figure 11. Evolution of α' martensite in isothermal constant amplitude fatigue tests with 0.5% total strain amplitude: (**a**) full range; (**b**) initial range.

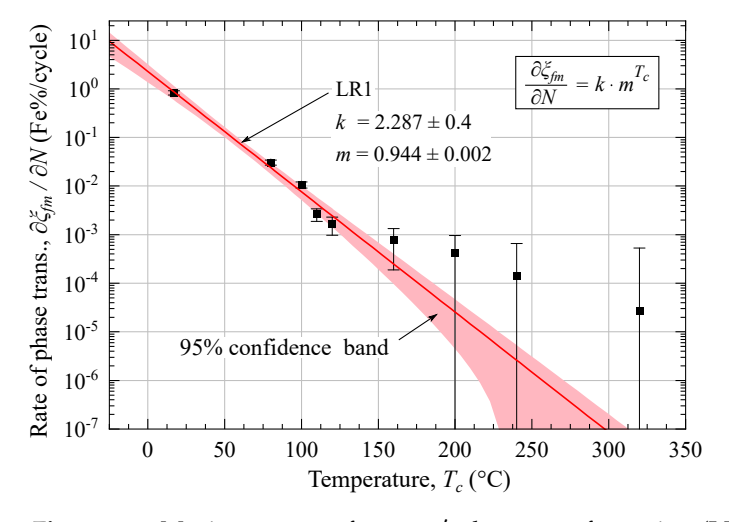


Figure 12. Maximum rate of $\gamma \to \alpha'$ phase transformation (LR1) at constant strain amplitude $\varepsilon_{a,t} = 0.5\%$ as a function of temperature.

Table 2. Parameters for linear approximation of the maximum rate of phase transformation (LR1) at elevated temperatures.

Temperature T_c , °C	Linear Range LR1 ξ_{fm} , Fe%	LR1 Slope Fe%/cycle	LR1 Normalized –
17	10.0–20.0	0.826	1
80	3.00–10.0	0.0305	0.0369

Table 2. Cont.

Temperature T_c , °C	Linear Range LR1 ξ_{fm} , Fe%	LR1 Slope Fe%/cycle	LR1 Normalized –
100	2.00-8.00	0.01066	0.0129
110	0.50-2.50	0.00264	0.0032
120	0.40-1.60	0.00163	0.00197
160	0.10-0.80	7.651×10^{-4}	9.26271×10^{-4}
200	0.08-0.50	$4.1803 imes 10^{-4}$	5.0609×10^{-4}
240	0.03-0.10	1.4172×10^{-4}	1.71574×10^{-4}
320	0.075-0.09	2.6433×10^{-5}	3.20012×10^{-5}

4. Discussion

Electrical resistance measurement during strain increase tests was conducted to determine the lowest strain amplitude at which the austenite lattice was affected. Electrical resistance (or conductivity) measurements are widely regarded as sensitive indicators of microstructural changes [18–22], as dislocation movements can occur in the early stages of fatigue and subsequently affect the mobility of valence electrons within the lattice. A strain increase test, with parameters identical to those described in Section 3.1, was performed, and electrical resistance was measured by the four-probe method. The only difference was the introduction of a load-free hold time of 60 min after every step. The temperature measured during the hold time T_{rst} is therefore named the hold temperature, and the temperature when the cyclic load was applied T_{cycle} —cycle temperature. Thermo-electric currents were compensated by subtracting the voltage drop without current continuously in 3-s intervals (3 s with power supply on, 3 s off).

From Figure 13, one can observe that electrical resistance first decreases from $\varepsilon_{a,p} = 0.09\%$ to 0.15% and only then starts to increase. This first change in electrical resistance corresponds very well to the first change in ferromagnetic volume fraction (see Figure 5a) that was observed at $\varepsilon_{a,p} = 0.10\%$. It can therefore be said that the cyclic strain limit of about 0.08% is valid for the given material at ambient temperature. This cyclic strain limit can potentially serve as a quick way of estimating the fatigue endurance limit.

Measured by a UMB, the ferromagnetic volume fraction ξ_{fm} represents an average value over the fatigue specimen gauge length, with only slightly higher surface sensitivity. However, the material itself is not entirely homogeneous, and a localized phase transformation could potentially take place. In order to check this hypothesis, MFI was used to map the spatial distribution of α' martensite in fatigue specimens after the constant amplitude tests described in Section 3.2. These results are presented in Figures 14 and 15.

All numerical values of MFI measurements represent the ferromagnetic volume fraction (or density), except for Figure 14a, where the amount of deformation-induced martensite exceeded the calibration table values and therefore has arbitrary units.

The most uniform distribution of α' martensite was observed following the isothermal test at 17 °C. At 80 °C, there was strong evidence of α' martensite forming in axial bands. In these bands, Fe% values reached up to 30%, while the surrounding troughs showed levels as low as 10%. At 100 °C, vertical bands were present as well, but a new trend also began to become apparent—a higher α' martensite volume in the transition region from the gauge to the shaft. In this transitional region, the ferrite content reading was 11%, while at the center of the gauge length, it was only 2.7%. This behavior could be linked to the increased shear deformation in these areas due to slight lateral movement of the fatigue specimen.

Compared to Figure 14, the colormap range in Figure 15 was reduced from 25 Fe% to 1.5 Fe%, since $\gamma \to \alpha'$ transformation at these temperatures was significantly reduced. Nevertheless, an increase in the Fe% reading of about 1.8% could be observed in the fatigue specimen after the 200 °C fatigue test (Figure 15a). Fatigue specimens tested at 240 °C and

320 °C showed a very similar quantity and distribution of α' martensite. There was only a slight increase of about 0.25 Fe% at the gauge length relative to the shoulders of the fatigue specimen. This increase is likely to be only indirectly related to the fatigue load. Since the specimen surface was first ground with sandpaper and then polished with 6, 4, and 1 μ m diamond suspension, it is possible that the stability of austenite was first affected by fatigue loading and then α' martensite developed at the gauge length by mechanical polishing.

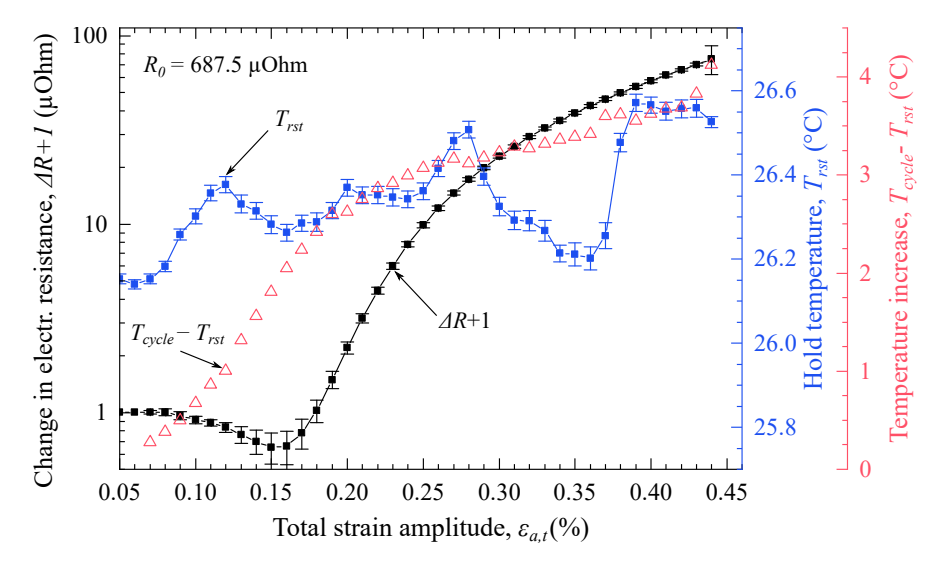


Figure 13. Electrical resistance as a function of strain amplitude in a SIT. Error bars show the scatter of values recorded during the hold period. Initial electrical resistance R_0 was subtracted while 1 μ Ohm was added to display negative values in a logarithmic scale.

The influence of surface flatness on MFI measurement was also considered. Due to the mechanical polishing, the surface of the sample had a slightly rounded shape, which resulted in a 3 to 4 μ m difference in working distance. After considering this, it was found that the change in working distance can only account for one-tenth of the ferromagnetic volume fraction difference between the gauge length and the shafts of the specimen in Figure 15.

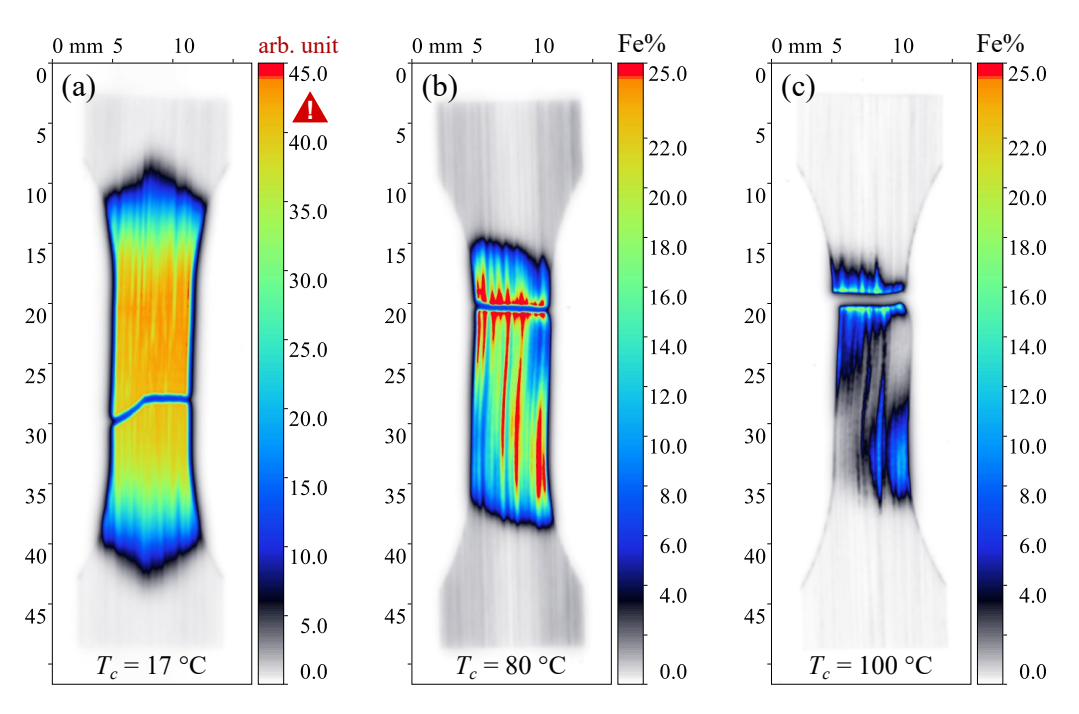


Figure 14. Cont.

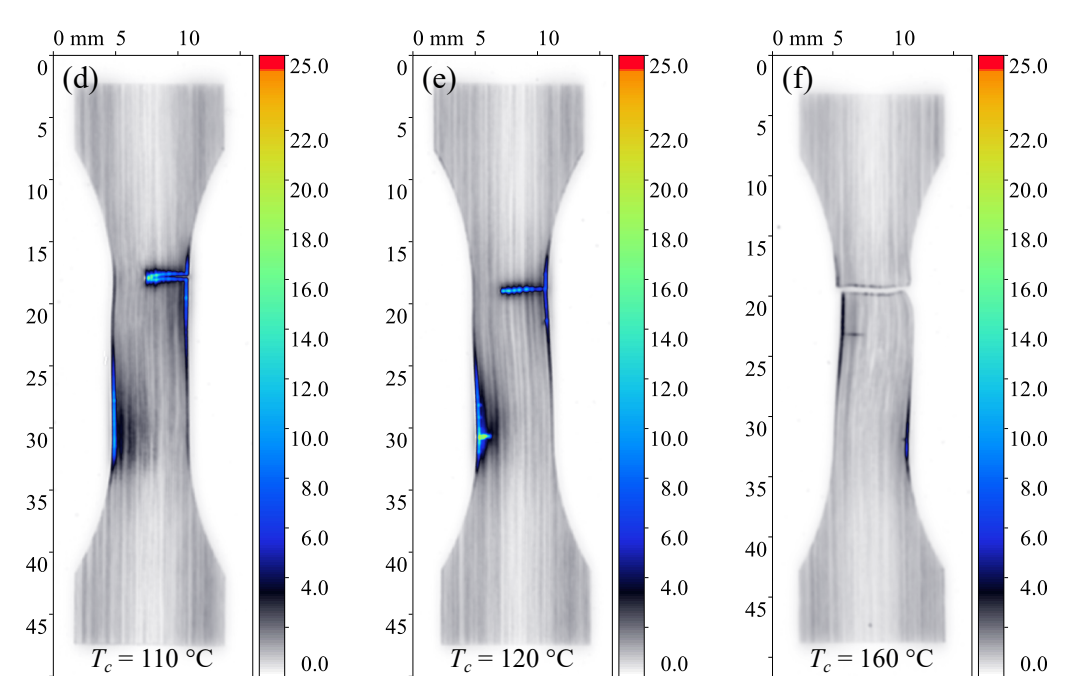


Figure 14. Results of magnetic force imaging (MFI) mapping of ferromagnetic volume fraction in Fe% after isothermal constant amplitude fatigue testing described in Section 3.2: (a) $T_c = 17$ °C; (b) $T_c = 80$ °C; (c) $T_c = 100$ °C; (d) $T_c = 110$ °C; (e) $T_c = 120$ °C; (f) $T_c = 160$ °C.

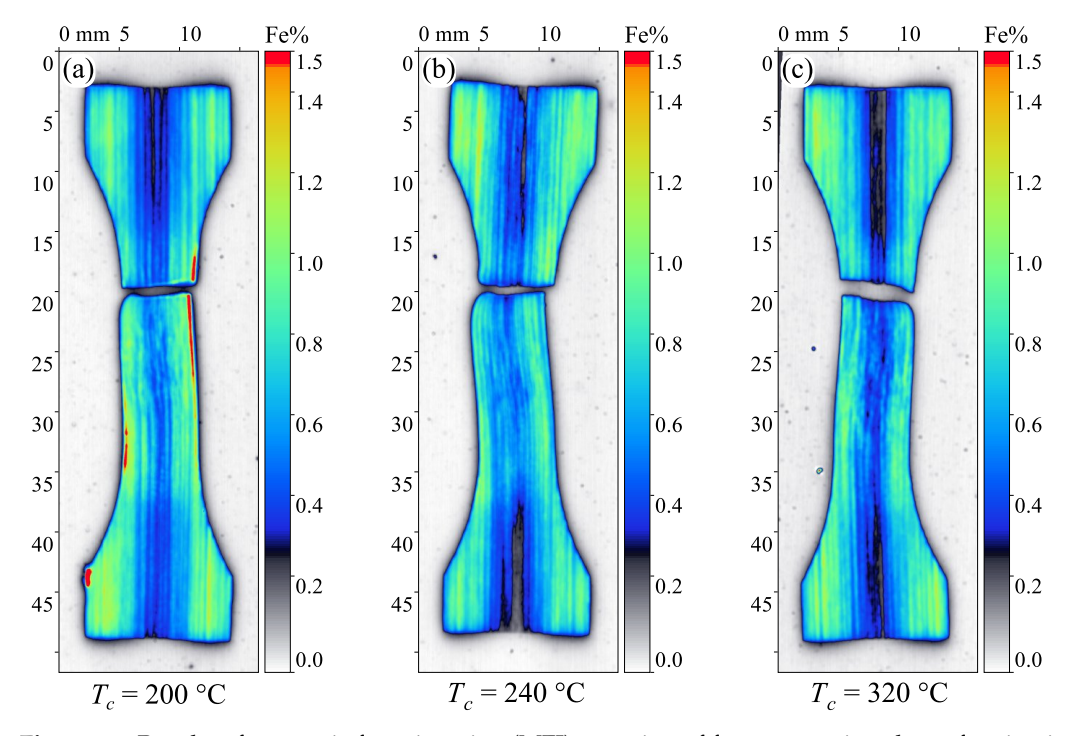


Figure 15. Results of magnetic force imaging (MFI) mapping of ferromagnetic volume fraction in Fe% after isothermal constant amplitude fatigue testing described in Section 3.2: (a) $T_c = 200 \,^{\circ}\text{C}$; (b) $T_c = 240 \,^{\circ}\text{C}$; (c) $T_c = 320 \,^{\circ}\text{C}$.

5. Conclusions

The experimental results presented in this paper demonstrate how the deformation-induced transition from austenite to martensite is affected by elevated temperatures. In situ magnetic and electrical resistance measurements during strain increase fatigue tests showed that a strain amplitude of 0.1% was already sufficient to form α' martensite at room tempera-

ture. At elevated temperatures, 240 °C appeared to be the transition temperature, at which less than 0.25 Fe% was measured, right until the specimen fracture at 0.22% strain amplitude.

The kinetics of $\gamma \to \alpha'$ transformation were further investigated in a series of isothermal constant amplitude fatigue tests. From this data, an empirical mathematical model was developed to describe the maximum rate of phase transformation. This model describes the kinetics of $\gamma \to \alpha'$ transformation as an exponential function of temperature, where the rate of phase transformation decreases with temperature, asymptotically approaching zero but never actually reaching it. The spatial distribution of α' martensite in isothermal fatigue tests played a significant role in how the volume fraction was estimated and requires further research where shear and uniaxial strains can be separated more clearly.

Author Contributions: Conceptualization, V.L.; methodology, V.L.; software, S.P.; validation, P.S. and C.B.; investigation, V.L.; resources, C.B.; data curation, V.L.; writing—original draft preparation, V.L.; writing—review and editing, P.S. and C.B.; visualization, V.L.; supervision, C.B. and P.S.; project administration, C.B.; funding acquisition, V.L. and C.B. The authors declare that generative artificial intelligence has not been used in this article, neither to generate text, data, or graphics nor to assist in the study, design, data collection, analysis, or interpretation. All authors have read and agreed to the published version of the manuscript.

Funding: This research was funded by the German Federal Ministry for the Environment, Nature Conservation, Nuclear Safety and Consumer Protection grant number 1501608, "ZeMess", "Zerstörungsfreie elektromagnetische und elektrische Messung betriebsbedingter Schädigung in mechanisch und thermisch beanspruchten austenitischen Stählen", "Non-destructive electromagnetic measurement of operational damage in thermo-mechanically stressed austenitic steels".

Institutional Review Board Statement: Not applicable.

Informed Consent Statement: Not applicable.

Acknowledgments: The financial support of the German Federal Ministry for the Environment, Nature Conservation, Nuclear Safety and Consumer Protection is gratefully acknowledged. The authors would also like to thank the Chair of Functional Materials of Saarland University, and C. Pauly personally, for microstructural investigations. Special thanks go to Gerd Dobmann for valuable comments and discussions.

Conflicts of Interest: The authors declare no conflicts of interest. The funders had no role in the design of the study; in the collection, analysis, or interpretation of data; in the writing of the manuscript; or in the decision to publish the results.

References

- Angel, T. Formation of martensite in austenitic stainless steels—Efect of deformation, temperature, and composition. *J. Iron Steel Inst.* 1954, 177, 165–174.
- 2. Voehringer, O.; Macherauch, E. Struktur und mechanische Eigenschaften von Martensit. *HTM—Haerterei-Tech. Mitteilungen* **1977**, 32, 153–168. [CrossRef]
- 3. Cohen, M.; Olson, G.B.; Clapp, P.C. On the classification of displacive phase transformations. In Proceedings of the International Conference on Martensitic Transformations, Cambridge, MA, USA, 24–29 June 1979.
- 4. Müller-Bollenhagen, C. Verformungsinduzierte Martensitbildung bei mehrstufiger Umformung und deren Nutzung zur Optimierung der HCF- und VHCF-Eigenschaften von austenitischem Edelstahlblech. Ph.D. Thesis, Universität Siegen, Siegen, Germany, 2011.
- 5. Bain, E.; Dunkirk, N. The nature of martensite. Trans. AIME 1924, 70, 25–45.
- 6. Kurdjumow, G.; Sachs, G. Über den Mechanismus der Stahlhärtung. Zeitschrift Phys. 1930, 64, 325–343. [CrossRef]
- 7. Nishiyama, Z. Strain-induced transformation in Co26Ni-8.7 Cr alloy. Sci. Rep. Tohoku Imp. Univ. 1934, 25, 94.
- 8. Pitsch, W. The martensite transformation in thin foils of iron-nitrogen alloys. *Philos. Mag. A J. Theor. Exp. Appl. Phys.* **1959**, 4,577–584. [CrossRef]
- 9. Bogers, A.J.; Burgers, W.G. Partial dislocations on the {110} planes in the B.C.C. lattice and the transition of the F.C.C. into the B.C.C. lattice. *Acta Metall.* **1964**, *12*, 255–261. [CrossRef]

10. Shin, H.C.; Ha, T.K.; Chang, Y.W. Kinetics of deformation induced martensitic transformation in a 304 stainless steel. *Scr. Mater.* **2001**, *45*, 823–829. [CrossRef]

- 11. Hänsel, A. Nichtisothermes Werkstoffmodell für die FE-Simulation von Blechumformprozessen mit Metastabilen Austenitischen CrNiStählen. Ph.D. Thesis, ETH Zürich, Zurich, Switzerland, 1998. [CrossRef]
- 12. Smaga, M.; Walther, F.; Eifler, D. Investigation and modelling of the plasticity-induced martensite formation in metastable austenites. *Int. J. Mater. Res.* **2006**, *97*, 1648–1655. [CrossRef]
- 13. Lang, M.; Johnson, J.; Schreiber, J.; Dobmann, G.; Bassler, H.J.; Eifler, D.; Ehrlich, R.; Gampe, U. Cyclic deformation behaviour of AISI 321 austenitic steel and its characterization by means of HTC-SQUID. *Nucl. Eng. Des.* **2000**, *198*, 185–191. [CrossRef]
- 14. Fischer Technology Inc. Feritscope FMP30; Fischer Technology Inc.: Windsor, CT, USA, 2022.
- 15. Lyamkin, V.; Pauly, C.; Starke, P.; Mücklich, F.; Boller, C. Impact of cyclic strain on deformation-induced martensite morphology and magnetic properties of type 347 austenitic stainless steel. *Mater. Today Commun.* **2021**, 26, 101803. [CrossRef]
- 16. Lyamkin, V.; Starke, P.; Boller, C. Magnetic force imaging for spatially resolved assessment of ferromagnetic phase fraction in austenitic stainless steel. *J. Magn. Magn. Mater.* **2019**, 497, 165973. [CrossRef]
- 17. Hotz, H.; Kirsch, B.; Aurich, J.C. Impact of the thermomechanical load on subsurface phase transformations during cryogenic turning of metastable austenitic steels. *J. Intell. Manuf.* **2020**, *32*, 877–894. [CrossRef]
- 18. Starke, P.; Walther, F.; Eifler, D. Fatigue assessment and fatigue life calculation of quenched and tempered SAE 4140 steel based on stress-strain hysteresis, temperature and electrical resistance measurements. *Fatigue Fract. Eng. Mater. Struct.* **2007**, 30, 1044–1051. [CrossRef]
- 19. Mai, J.; Peng, L.; Lin, Z.; Lai, X. Experimental study of electrical resistivity and flow stress of stainless steel 316L in electroplastic deformation. *Mater. Sci. Eng. A* **2011**, *528*, 3539–3544. [CrossRef]
- 20. Omari, M.A.; Sevostianov, I. Estimation of changes in the mechanical properties of stainless steel subjected to fatigue loading via electrical resistance monitoring. *Int. J. Eng. Sci.* **2013**, *65*, 40–48. [CrossRef]
- 21. Starke, P.; Walther, F. Model-based correlation between the electrical resistance and the dislocation structure of the fatigue-loaded ICE-railway wheel steel R7. *Mater. Test.* **2015**, *57*, 9–16. [CrossRef]
- 22. Knobbe, H.; Starke, P.; Herenu, S.; Christ, H.J.; Eifler, D. Cyclic deformation behaviour, microstructural evolution and fatigue life of duplex steel AISI 329 LN. *Int. J. Fatigue* **2015**, *80*, 81–89. [CrossRef]

Disclaimer/Publisher's Note: The statements, opinions and data contained in all publications are solely those of the individual author(s) and contributor(s) and not of MDPI and/or the editor(s). MDPI and/or the editor(s) disclaim responsibility for any injury to people or property resulting from any ideas, methods, instructions or products referred to in the content.